

Scaling analysis of normal state properties of high temperature superconductors

H. G. Luo¹, Y. H. Su², and T. Xiang^{3,1}

¹*Institute of Theoretical Physics, Chinese Academy of Sciences, P.O. Box 2735, Beijing 100080, China*

²*Department of Physics, Yantai University, Yantai 264005, China and*

³*Institute of Physics, Chinese Academy of Sciences, P.O. Box 603, Beijing 100080, China*

We propose a model-independent scaling method to study the physical properties of high temperature superconductors in the normal state. We have analyzed the experimental data of the c-axis resistivity, the in-plane resistivity, the Hall coefficient, the magnetic susceptibility, the spin-lattice relaxation rate, and the thermoelectric power using this method. It is shown that all these physical quantities exhibit good scaling behaviors, controlled purely by the pseudogap energy scale in the normal state. The doping dependence of the pseudogap obtained from this scaling analysis agrees with the experimental results of angle-resolved photoemission and other measurements. It sheds light on the understanding of the basic electronic structure of high- T_c oxides.

I. INTRODUCTION

The mechanism of high- T_c superconductivity remains one of the fundamental issues unsolved in condensed matter physics. In particular, a unified theory towards the understanding of the rich phase diagram of high- T_c superconductors (HTSC) has not been established. At half filling, the parent compounds of HTSC are antiferromagnetic insulators. Upon doping, the antiferromagnetic long range correlation is suppressed and the high- T_c superconductivity develops above a critical doping level. At low doping but in the metallic state, a pseudogap phase with missing entropy or spectra, is discovered.¹ Around the optimal doping, a strange metal phase with a linear in-plane resistivity and probably a quantum critical point emerges.² In the heavily overdoped regime, the conventional Landau Fermi liquid behaviors are gradually recovered. Throughout the whole doping range, the electron states seem to be intrinsically inhomogeneous.³

A must step in the understanding of the phase diagram of HTSC is to identify the energy scales and the control parameters or interactions of low energy excitations of HTSC. In the normal state at low doping, the pseudogap is believed to be one of the characteristic parameters of low-lying excitations. The corresponding temperature below which the pseudogap effect is observed is commonly used as a boundary to separate the pseudogap and the strange metal phases, although there is no real phase transition between these phases. However, due to the uncertainty in the definition of the pseudogap, different experiments have adopted different criteria to determine the pseudogap energy scale. This leads to the claim of the existence of two pseudogaps, namely the upper and lower pseudogaps.⁴ In the strange metal phase, the quantum critical fluctuation is strong and the temperature itself may serve as a dynamic control parameter as suggested by the marginal Fermi liquid theory.⁵

The scaling analysis of experimental data in HTSC is a simple but powerful tool in elucidating the underlying physics without invoking a specific model. In the normal state, if the pseudogap is a predominant energy scale controlling low-energy excitations, then the low temperature

behavior of any measurement physical quantity should satisfy a doping-independent scaling law, although the analytic expression of the scaling function is unknown. Based on this idea, we analyzed recently the temperature dependence of the c-axis resistivity ρ_c of HTSC and found that it obeys a universal scaling law given by⁶

$$\rho_c(T) = \frac{\alpha T}{\Delta} \exp\left(\frac{\Delta}{T}\right), \quad (1)$$

where α is a doping dependent coefficient, T is temperature and Δ is the pseudogap. As shown in Ref. [6], Eq. (1) results from the interplay between the anisotropic c-axis hopping integral^{7,8} and the $d_{x^2-y^2}$ -like symmetry of the pseudogap. It agrees excellently with the experimental data of multi-layer HTSC and resolved a long-standing puzzle regarding the physical origin of the semiconductor-like temperature dependence of ρ_c in the pseudogap phase. Furthermore, it suggests that there is only one energy scale controlling the low-energy excitations around the antinodal points and the interlayer hopping within each unit cell is coherent.

However, if the scaling function is unknown, the scaling analysis becomes difficult. This has in fact hampered the application of the scaling analysis. A commonly adopted approach in the scaling analysis in the literature is to assume that by normalizing both the measurement quantity $F(T)$ and the temperature by the corresponding values at a sample-dependent characteristic temperature T^* , then all the experimental data should fall onto a single curve described by the scaling function

$$\frac{F(T)}{F(T^*)} = g\left(\frac{T}{T^*}\right). \quad (2)$$

However, in real materials, this scaling analysis often fails since $F(T)$ generally contains the terms which are not scaling invariant. For example, the impurity contribution to the in-plane resistivity or other physical quantities, is not scaling variant. Moreover, since T^* is unknown prior to the analysis, this formula is difficult to be implemented practically even if it is correct. Empirically, T^* is often determined from some special features appeared in the measurement data. For example, for the

in-plane resistivity, T^* is determined from the temperature below which the resistivity begins to deviate from its high temperature linear-T behavior. However, to determine unambiguously the linear-T region is not always possible since in some low doping samples, the measured temperature may not be high enough to reach the linear T regime. Furthermore, the deviation from linear to nonlinear T is a crossover, not a phase transition, a small measurement error may result in a large error in T^* .

In this paper we propose a novel scaling method and apply it to analyze the normal state properties of HTSC. This method extends our previous scaling analysis of the c-axis resistivity to other physical quantities. It breaks the barrier in the use of the simple formula (2) and allows a model independent scaling analysis to be done reliably. We have reanalyzed the experimental data of the c-axis resistivity of HTSC with this method. By comparison with our previous results,⁶ we find that this method indeed works very well. It provides a simple but powerful approach for analyzing experimental results. Furthermore, this method is model independent. It can be applied not only to the high- T_c cuprates, but also to any other materials where the single parameter scaling behavior is valid.

This paper is arranged as follows. Sec. II gives an introduction to the scaling method based on a least square fit of an unknown scaling function to the experimental data. In Sec. III, we apply the method to analyze the scaling behaviors of a number of physical quantities of HTSC in the normal state, using the experimental data published in the literature. In Sec. IV, we analyze the universal behavior of the energy scales obtained in Sec. III and discuss its physical implications. Sec. V gives a brief summary.

II. METHOD OF SCALING ANALYSIS

In this section, we present a generic method for analyzing the scaling behavior of a set of experimental data $\{F_i(T), i = 1 \dots N\}$. Here T can be a temperature, pressure, external field or any other controllable variable used in experiments. The subscript i is a sample index to which the physical quantity F as a function of T is measured experimentally. N is the total number of samples. In the discussion below, in order to be directly relevant to the scaling analysis presented in Sec. III, we assume that T is the temperature and a sample represents a specified high- T_c compound.

We start by assuming that in a relevant temperature range the low-lying physics is governed only by one energy scale Δ . Thus the measured physical quantity $F(T)$ satisfies a simple scaling law

$$F(T) = \alpha \mathcal{F}\left(\frac{T}{\Delta}\right) + \beta, \quad (3)$$

where α , β and Δ are all doping dependent but temperature independent. For the physical quantities to be dis-

cussed in Sec. III, β is generally the contribution of impurities or other extrinsic interactions. Δ is a characteristic energy scale of the system. It controls the dynamics of the system. $\mathcal{F}(T)$ is a universal (doping-independent) scaling function. Its temperature dependence is determined by the low-lying excitations and interactions.

The scaling function $\mathcal{F}(T)$ is generally unknown. This is the difficulty commonly met in the data analysis. However, the scaling method introduced here does not depend on the detailed formula of $\mathcal{F}(T)$, provided that the single-parameter scaling hypothesis Eq. (3) is valid. This is a merit of the method. It provides a simple but powerful approach to probe the intrinsic connection between different samples and to determine the doping dependence of the characteristic energy scale Δ without invoking a specific model.

The aim of the scaling analysis is to determine from the measurement data the scaling parameters, $(\alpha_i, \Delta_i, \beta_i)$, and the optimized scaling functions $\mathcal{F}(x)$ so that all the data can be rescaled onto a universal curve. This can in principle be achieved by minimizing the total deviation of the scaling function between any two samples:

$$\delta\mathcal{F} = \sum_{i < j}^N \sum_k^{N_k} [\mathcal{F}_i(T'_k) - \mathcal{F}_j(T'_k)]^2, \quad (4)$$

where

$$\mathcal{F}_i(T) = \frac{1}{\alpha_i} [F_i(\Delta_i T) - \beta_i]. \quad (5)$$

$F_i(\Delta_i T)$ is the value of F of the i -th sample at temperature $\Delta_i T$. N_k is the number of sampled temperature points used in optimizing the scaling function. N_k can be adjusted in the minimization. Initially, N_k can take roughly the value of average measured temperature points.

However, due to the scaling behavior of $\mathcal{F}(T)$, not all the parameters $(\alpha_i, \Delta_i, \beta_i)$ can be uniquely determined by the minimization of $\delta\mathcal{F}$ if \mathcal{F} is unknown. Indeed, from Eqs. (4) and (5), it can be shown that if $\{\alpha_i, \Delta_i, \beta_i\}$ ($i = 1 \dots N$) is a set of parameters minimizing $\delta\mathcal{F}$, then $(\alpha_i/\alpha_s, \Delta_i/\Delta_s, \beta_i - \beta_s\alpha_i/\alpha_s)$ with arbitrary but non-singular $(\alpha_s, \Delta_s, \beta_s)$ will also minimize $\delta\mathcal{F}$. $(\alpha_s, \Delta_s, \beta_s)$ are unknown and can be taken as the scaling parameters of a reference sample. This means that only the relative values of α_i , Δ_i , and β_i with respect to a reference sample

$$A_i = \frac{\alpha_i}{\alpha_s}, \quad (6)$$

$$B_i = \frac{\Delta_i}{\Delta_s}, \quad (7)$$

$$C_i = \beta_i - A_i\beta_s, \quad (8)$$

can be fixed. From the definitions (6-8), it is straightforward to show that $A_s = B_s = 1$, $C_s = 0$.

Using the relative scaling parameters (A_i, B_i, C_i) , one can define a new scaling function

$$f\left(\frac{T}{B}\right) = \alpha_s \mathcal{F}\left(\frac{T}{B\Delta_s}\right) + \beta_s. \quad (9)$$

$F(T)$ can then be expressed as

$$F(T) = A f\left(\frac{T}{B}\right) + C. \quad (10)$$

For the reference sample, the scaling function is the measurement curve itself: $F(T) = f(T)$.

Eq. (10) is nothing but to scale all experimental data onto the measurement curve of the reference sample. This suggests that the reference sample should be chosen such that its temperature interval is broad enough to cover the whole temperature range physically interesting and the data quality is among one of the best.

The relative scaling parameters $\{A_i, B_i, C_i\}$ can now be determined by minimizing the total deviation of the scaling functions:

$$\delta f = \sum_{i < j}^N \sum_k^{N_k} [f_i(T_k) - f_j(T_k)]^2, \quad (11)$$

where

$$f_i(T) = \frac{1}{A_i} [F_i(B_i T) - C_i], \quad (12)$$

In general, $B_i T$ may not be exactly the temperature point experimentally measured. The value of $F_i(B_i T)$ can be obtained from the measurement data by interpolation, provided that $B_i T$ is within the measured temperature interval. For each pair of f_i and f_j , if $B_i T_k$ or $B_j T_k$ is outside the measured temperature interval for the i 'th or j 'th sample, then the corresponding term in Eq. (4) should be excluded from the summation. The minimization of δf can be done, for example, using the standard subroutine given in *Numerical Recipes*.⁹

TABLE I: The scaling parameters for the in-plane resistivity ρ_{ab} of $\text{YBa}_2\text{Cu}_3\text{O}_{6+\delta}$ published by Ito et al.¹⁰ The parameters of the reference sample, $\delta = 0.68$, are bold faced.

sample (δ)	A	B	C ($10^{-4}\Omega\text{cm}$)
0.68	1.0	1.0	0.0
0.78	0.63	0.81	0.0074
0.85	0.39	0.60	-0.10

Below we take the in-plane resistivity data of $\text{YBa}_2\text{Cu}_3\text{O}_{6+\delta}$ published by Ito et al.¹⁰ as an example to show how the method works. For simplicity, here we only use the experimental data for three of the samples, $\delta = (0.68, 0.78, 0.85)$. Fig. 1(a) shows the measurement data of $\rho_{ab}(T)$ for these three samples. In the scaling analysis, we take $\delta = 0.68$ as the reference sample and N_k

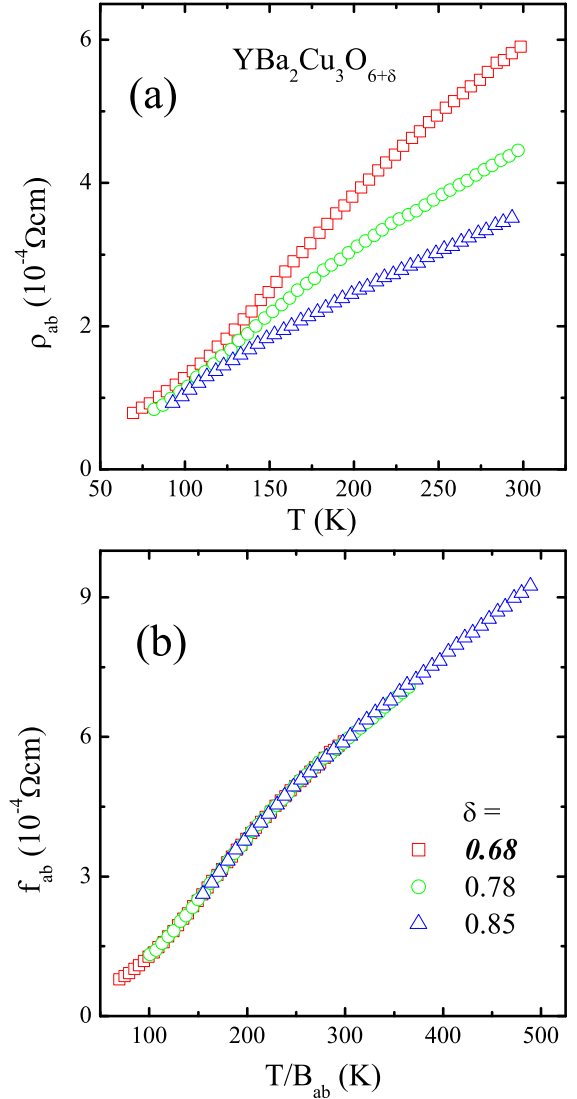


FIG. 1: (a) The experimental data of the in-plane resistivity $\rho_{ab}(T)$ of $\text{YBa}_2\text{Cu}_3\text{O}_{6+\delta}$, extracted from Fig. 2(a) of Ref. [10]. (b) The scaling plot of the experimental data. The reference sample is $\delta = 0.68$.

to be roughly equal to the measured temperature points of the reference sample. The relative scaling parameters can then be determined by numerically minimizing Eq. (11). The resulting scaling curves are shown in Fig. 1(b) and the scaling parameters are given in Table I.

In Eq. (10), if $C \ll F(T)$, then the scaling equation is approximately given by

$$F(T) \approx A f\left(\frac{T}{B}\right). \quad (13)$$

In this case, the scaling equation can be reexpressed as

$$\frac{F(T)}{F(T')} = \frac{f(T/B)}{f(T^*/B)} \equiv g\left(\frac{T}{T^*}\right), \quad (14)$$

where T' is a sample-dependent characteristic temperature. $g(T)$ is a rescaled function of $f(T)$. Eq. (14) is precisely the scaling equation defined by Eq. (2). It is a commonly used scaling equation in the scaling analysis of experimental data. However, it should be pointed out that this equation is valid only when the temperature independent term C can be safely ignored or reliably subtracted from $F(T)$ in Eq. (10).

III. SCALING ANALYSIS OF EXPERIMENTAL DATA

In this section, we apply the scaling method to analyze the experimental data of high T_c cuprates in the normal state. We will first analyze the scaling behavior of the c-axis resistivity ρ_c . Since an approximate but accurate expression for the scaling function of ρ_c is available, this allows us to determine the absolute values of the scaling parameters. For other measurement quantities, including the in-plane resistivity $\rho_{ab}(T)$, the Hall coefficient $R_H(T)$, the magnetic susceptibility $\chi(T)$, the spin-lattice relaxation rate $1/T_1T$ and the thermoelectric power $S(T)$, only the relative scaling parameters can be determined.

Our scaling analysis is based on the experimental data already published in the literature. We collect as much as we can the experimental data of HTSC from which a systematical analysis of the scaling behaviors can be done. The preference is given to the latest published data if there are considerable difference between the data published by different groups. The chemical formula of the compounds with their abbreviations analyzed in this paper are given in Table II. The scaling analysis here will be limited to the superconducting samples in the normal state. The data for the non-superconducting samples will not be analyzed. In all figures and tables presented in this paper, the parameters for the reference samples will be the bold faced to distinguish from other parameters.

In the comparison of the scaling parameters for different families of HTSC, we will use the superconducting transition temperature T_c and its empirical formula proposed by Presland et al.¹¹

$$\frac{T_c}{T_{c,max}} = 1 - 82.6(p - 0.16)^2 \quad (15)$$

to determine the effective carrier concentration p . Here $T_{c,max}$ is the maximal superconducting transition temperature. For $\text{La}_{2-x}\text{Sr}_x\text{CuO}_4$, the carrier concentration is equal to the doping concentration of Sr ions, $p = x$.

TABLE II: HTSC compounds and their abbreviations analyzed in this paper.

$\text{YBa}_2\text{Cu}_3\text{O}_{6+\delta}$	Y123
$\text{Y}_{0.8}\text{Ca}_{0.2}\text{Ba}_2\text{Cu}_3\text{O}_{6+\delta}$	Ca-Y123
$\text{YBa}_2\text{Cu}_4\text{O}_8$	Y124
$\text{Bi}_2\text{Sr}_2\text{CaCu}_2\text{O}_{8+\delta}$	Bi2212
$\text{Bi}_2\text{Sr}_2\text{Ca}_2\text{Cu}_3\text{O}_{10+\delta}$	Bi2223
$\text{La}_{2-x}\text{Sr}_{2-x}\text{CuO}_4$	La214
$\text{Bi}_2\text{Sr}_{2-x}\text{La}_x\text{CuO}_{6+\delta}$	La-Bi2201
$\text{HgBa}_2\text{CuO}_4$	Hg1201
$\text{TlSr}_2\text{CaCu}_2\text{O}_{7-\delta}$	Tl1212

A. The c-axis resistivity $\rho_c(T)$

In the pseudogap phase of high- T_c cuprates, the c-axis resistivity ρ_c behaves very differently from its in-plane counterpart ρ_{ab} . Along the CuO_2 plane, ρ_{ab} shows a metal-like temperature dependence. It decreases with decreasing temperature. However, along the c-axis, ρ_c behaves as a semiconductor. It increases with decreasing temperature.

This dramatic difference between ρ_c and ρ_{ab} is not what one might expect within conventional Fermi liquid theory. To resolve this issue, a number of theoretical models based on the dynamic confinement of charge-spin separated particles^{12,13,14} or the incoherent interlayer hopping^{15,16} were proposed. Most of the theories predicted that ρ_c should diverge in a certain power law of T at low temperature. However, it seems that none of these theories can account quantitatively or even qualitatively the experimental data.

The semiconductor-like behavior of ρ_c results, as we recently pointed out,⁶ from the interplay between the $d_{x^2-y^2}$ -like pseudogap and the anisotropic c-axis hopping integral.^{7,8} ρ_c contributes mainly from the quasiparticles around the antinodal points. The nodal contribution is completely suppressed by the interlayer hopping matrix elements. Since the pseudogap is a prevailing energy scale governing the c-axis dynamics in the pseudogap phase, it is natural to assume that the c-axis resistivity satisfies a scaling law governed purely by the pseudogap Δ .

In cuprate superconductors, if Cu atoms in the two neighboring CuO_2 planes lie collinearly along the c-axis, then the interlayer hopping integral between these two planes is given by

$$t_c \sim (\cos k_x - \cos k_y)^2, \quad (16)$$

where (k_x, k_y) are the in-plane momenta of electrons. t_c vanishes along the nodal direction. Based on this formula, we showed in Ref. [6] that for multilayer cuprates ρ_c is approximately given by

$$\rho_c(T) = \alpha \mathcal{F}_c \left(\frac{T}{\Delta} \right), \quad (17)$$

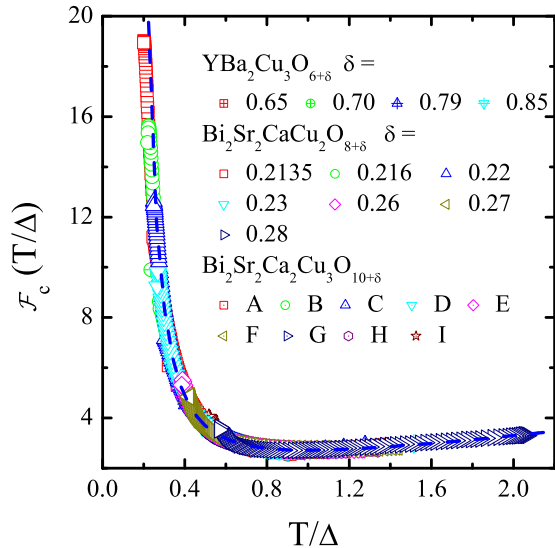


FIG. 2: The scaling function \mathcal{F}_c of the c-axis resistivity $\rho_c(T)$ for Y123, Bi2212 and Bi2223, compared with the theoretical curve determined by Eq. (18) (dashed line). The experimental data are obtained from Refs. [17,18,19] for Bi2212, Refs. [20] for Bi2223, and [21,22] for Y123. Bi2223 samples are labelled with the notations defined in Ref. [20].

where

$$\mathcal{F}_c(x) = x \exp\left(\frac{1}{x}\right). \quad (18)$$

Eq. (17) is a special case of Eq. (3). It holds when the residual resistivity contributed by disorder scattering β is vanishingly small compared with the contribution of pseudogap to ρ_c .

The scaling function (18), as shown in Fig. 2, agrees excellently with the measurement data for Y123 published by Yan et al.²¹ and by Babic et al.²² for Bi2212 by Watanabe et al.^{17,18,19} and for Bi2223 by Fujii et al.²⁰

The values of the scaling parameters α and Δ are given in Ref. [6]. The pseudogap Δ , as shown in Fig. (3), drops almost linearly with doping. This doping dependence of the pseudogap agrees with the angle-resolved photoemission (ARPES)⁶ as well as other measurement data.^{24,25} The values of Δ (not shown here) for two overdoped samples of Bi2212 from Chen et al.²⁶ deviate obviously from the other points. However, their ρ_c data can be well scaled onto the universal curve, as shown in Fig. 3(a) in Ref. [6]. A probable explanation is that the true doping levels for these two samples may not as high as reported. The four samples, F, G, H and I, of Bi2223 near optimal doping (here we adopt the notations used in Ref. 20), have almost the same T_c . However, their Δ obtained from ρ_c are very different. This might be due to the inhomogeneity of charge carriers in these samples, since T_c

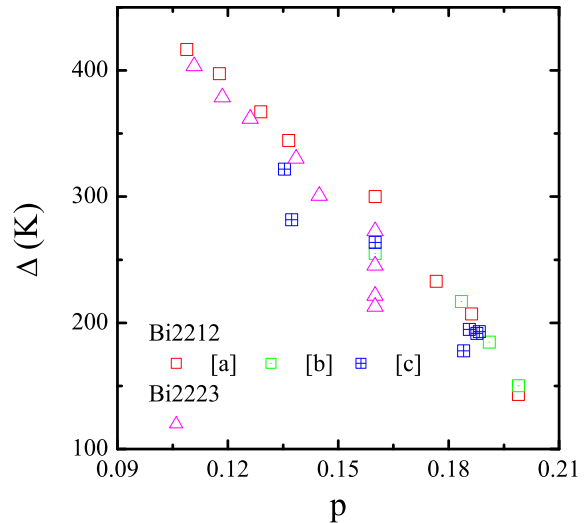


FIG. 3: The doping dependence of the pseudogap Δ obtained from the scaling analysis of the experimental data shown in Fig. 2 with Eqs. (17) and (18). [a], [b], and [c] refer to Ref. [17], [18,19] and [23], respectively.

is determined mainly by the fraction of a sample where the carrier concentration is close to the optimal doping, while ρ_c is the contribution of the whole sample.

The existence of the universal scaling law of ρ_c , especially its activated behavior, implies that the c-axis hopping is predominantly coherent, rather than incoherent as usually believed. The reason is actually simply. If the interlayer hopping is incoherent, then the excitations around the gap nodes may have substantial contribution to ρ_c , which may break this scaling law. For multiple layer cuprates, the intralayer coupling may be different to the interlayer coupling. However, the different coupling between CuO₂ planes does not change the fact that the pseudogap is the only energy scale governing the quasiparticle excitations around the antinodes in the normal state. Therefore, Eq. (17) holds irrespective of the number of CuO₂ planes in each unit cell.

TABLE III: The scaling parameters, A_c and B_c , of the c-axis resistivity ρ_c defined by Eq. (20) for La-Bi2201. The experimental data and the carrier concentration p are taken from Ref. [27].

sample (x)	T_c (K)	doping (p)	A_c	B_c
0.84	1.4	0.10	2.50	1.13
0.73	14	0.11	1.37	1.14
0.66	23	0.12	1.0	1.0
0.49	31	0.14	0.79	0.51
0.39	38	0.16	0.67	0.41

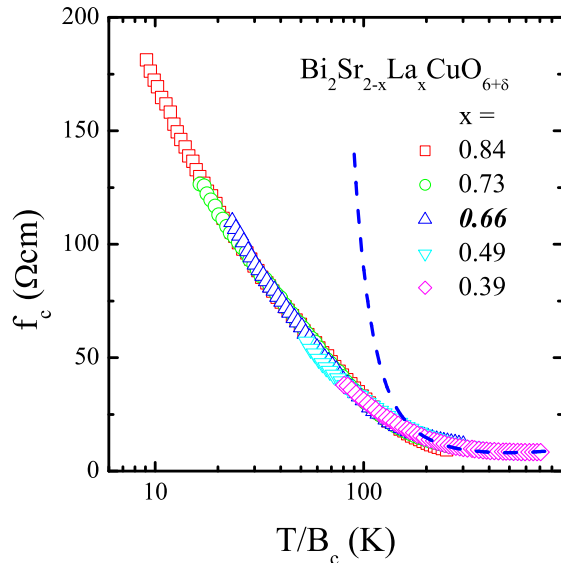


FIG. 4: Scaling behavior of the c-axis resistivity $\rho_c(T)$ for the single-layer cuprate superconductor La-Bi2201. The experimental data were taken from Ref. [27]. The dashed line denotes the scaling function defined by Eq. (18).

The above scaling analysis is done based on Eq. (18) by assuming that the interlayer hopping integral is given by Eq. (16). However, in single-layer cuprate compounds, Cu atoms of two adjacent CuO₂ planes do not lie collinearly along the c-axis. In this case, the c-axis hopping integral becomes⁸

$$t_c \sim (\cos k_x - \cos k_y)^2 \cos \frac{k_x}{2} \cos \frac{k_y}{2}. \quad (19)$$

B. The in-plane resistivity $\rho_{ab}(T)$

In contrast to the semiconductor-like behavior of ρ_c , the in-plane resistivity ρ_{ab} of high-T_c cuprate superconductors is metal-like in the normal state. In the under- and optimally doped materials, ρ_{ab} exhibits a universal linear behavior in high temperatures.³¹ The phonon-scattering can lead to a linear resistivity. However, the Debye temperature determined by applying the Bloch-Grüneisen formula is too low to account for the experimental data of Bi2201.³² The linear behavior of ρ_{ab} could be a manifestation of strong correlations. It is a characteristic behavior of marginal Fermi liquid,⁵ where the inelastic scattering rate scales linearly with temperature. It may also result from gauge^{33,34,35} or quantum critical

fluctuations. It vanishes along both the nodal and antinodal directions. The c-axis hopping thus contributes mainly from the low-lying excitations between the nodal and antinodal points. As the pseudogap is the dominant energy scale in the pseudogap phase, the scaling law of the c-axis resistivity, Eq. (17), should still hold. However, the scaling function of the single-layer cuprates is expected to be different. In this case, an accurate expression for the scaling function is not available. Thus we are unable to determine the absolute values of the scaling parameters Δ and α from the scaling analysis. However, the relative scaling parameters can be determined using the scaling method introduced in the previous section.

We have analyzed the scaling behavior of ρ_c for La-Bi2201 (Ref. [27]) using the formula

$$\rho_c = A_c f_c \left(\frac{T}{B_c} \right). \quad (20)$$

Again the contribution from impurity scattering to ρ_c is ignored since it is much smaller than the contribution from the pseudogap effect.

Fig. 4 shows the scaling function f_c for La-Bi2201. The scaling parameters are given in Table III. The analysis shows that ρ_c indeed exhibits a good scaling behavior in this one-layer material. However, the scaling function is different from that for the multilayer materials in low temperatures. It is also different from the logarithmic divergence behavior as observed by Ando et al. in La214 cuprates.²⁸

The scaling behavior of ρ_c for both the single- and multiple-layer cuprates indicates that the interlayer dynamics is indeed governed by the interplay between the anisotropic interlayer hopping integral and the pseudogap effect in all high-T_c cuprates.

fluctuations.

Below a characteristic temperature T^* , ρ_{ab} begins to deviate from the linear behavior. This deviation is correlated with the pseudogap effect and T^* is believed to be the onset temperature below which the pseudogap opens. However, the opening of the pseudogap does not lead to a phase transition. There are no thermal anomalies observed in the specific heat or other thermodynamic quantities around T^* .

To analyze the scaling behavior of the in-plane resistivity, we assume ρ_{ab} to satisfy the following scaling law

$$\rho_{ab}(T) = A_{ab} f_{ab} \left(\frac{T}{B_{ab}} \right) + C_{ab}. \quad (21)$$

Here the residual resistivity C_{ab} should be retained since

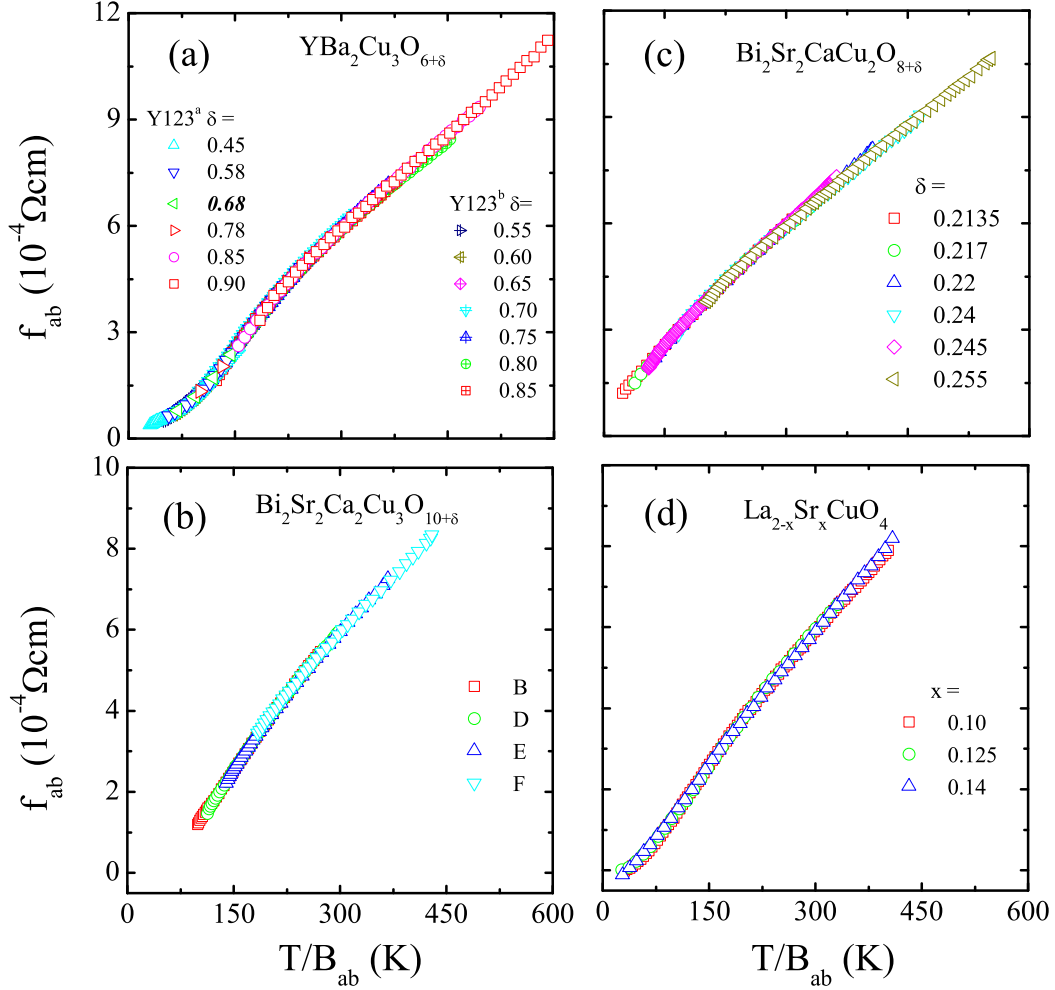


FIG. 5: The scaling function of the in-plane resistivity for Y123^a (Ref. [10]), Y123^b (Ref. [29]), Bi2212 (Ref. [17]), Bi2223 (Ref. [20]), and La214 (Ref. [30]). The Bi2223 samples are labeled using the notations given in Ref. [20].

the impurity contribution to ρ_{ab} is no longer negligible compared with the inelastic contribution of electrons to ρ_{ab} .

We have applied Eq. (21) to the experimental data published by Ito et al.¹⁰ for Y123, by Watanabe et al.¹⁷ for Bi2212, by Fujii et al.²⁰ for Bi2223, and by Nakano *et al.*³⁰ for La214. Fig. 5 shows the scaling function for these compounds. The corresponding scaling parameters are shown in Table IV. The measurement data (not shown in the figure) begin to deviate from the universal scaling curves near T_c due to superconducting fluctuations.

The result of Fig. 5 shows that ρ_{ab} indeed satisfies the simple scaling law described by Eq. (21). Moreover, all the curves shown in Fig. (5) are obtained by taking

Y123 $\delta = 0.68$ as a reference. This means that ρ_{ab} can be scaled onto a single curve for all these materials. Thus the scaling function of ρ_{ab} is universal. It does not depend on the chemical structure, nor neither on the doping level. This suggests that the in-plane resistivity is governed by the same scattering mechanism in all cuprate superconductors

The striking scaling behavior of ρ_{ab} indicates that the characteristic temperature T^* above which ρ_{ab} varies linearly with temperature is proportional to the scaling parameter B_{ab} . In Ref. [6], we showed that T^* is proportional to the pseudogap Δ determined from the c-axis resistivity within measurement errors, independent on doping. Thus B_{ab} is also proportional to Δ . This means that, same as for the c-axis resistivity, the pseudogap Δ

TABLE IV: The scaling parameters, A_{ab} , B_{ab} and C_{ab} for the in-plane resistivity of Y123^a (Ref. [10]), Y123^b (Ref. [29]) Bi2212 (Ref. [17]), Bi2223 (Ref. [20]), and La214 (Ref. [30]) as shown in Fig. 5. The notations used in Ref. [20] are adopted to label the samples of Bi2223. Y123^a with $\delta = 0.68$ is taken as the reference sample. The unit of C_{ab} is $10^{-4}\Omega\text{cm}$. The doping p of Y123^a, Bi2212 and Bi2223 are obtained from the empirical formula Eq. (15) with the maximum T_c being 93.54K for $\delta = 0.90$ of Y123^a, 89.0K for Bi2212 at $\delta = 0.22$ and 108.0K for F sample of Bi2223. The values of T_c for La214, Y123^a, Bi2212 and Bi2223 are obtained from Ref. [1, 10, 17, 20], respectively.

	sample	T_c (K)	doping (p)	A_{ab}	B_{ab}	C_{ab}
Y123 ^a	0.45	54.96	0.088	3.83	1.91	0.09
	0.58	64.67	0.098	1.48	1.22	0.13
	0.68	67.04	0.100	1.0	1.0	0.0
	0.78	80.26	0.118	0.63	0.81	0.0074
	0.85	92.08	0.146	0.39	0.60	-0.10
	0.90	93.54	0.16	0.22	0.50	-0.19
Y123 ^b	0.55			2.02	1.33	0.19
	0.60			1.57	1.20	-0.31
	0.65			1.35	1.15	-0.22
	0.70			0.89	0.92	-0.095
	0.75			0.70	0.81	-0.070
	0.80			0.55	0.65	-0.26
	0.85			0.52	0.78	0.049
Bi2212	0.2135	71.0	0.11	1.18	0.96	1.70
	0.217	77.0	0.119	1.07	0.89	1.10
	0.22	83.0	0.131	0.65	0.73	1.12
	0.24	89.0	0.16	0.51	0.63	0.60
	0.245	87.86	0.173	0.48	0.82	0.76
	0.255	87.4	0.175	0.32	0.54	0.24
Bi2223	B	93.0	0.118	0.12	1.09	0.31
	D	104.0	0.139	0.10	0.99	-0.20
	E	106.0	0.145	0.087	0.81	-0.69
	F	108.0	0.16	0.07	0.69	-0.90
La214	0.10	30.75	0.10	0.84	2.06	9.47
	0.125	32.0	0.125	0.60	1.97	6.93
	0.14	36.62	0.14	0.51	2.05	5.77

is also a control energy scale for the in-plane resistivity, although ρ_{ab} is mainly the contribution of nodal quasi-particle excitations.

Wuyts et al.^{36,37} did a similar scaling analysis for the in-plane resistivity of Y123. However, the characteristic temperatures (or energy scales) they determined are not very accurate. Their scaling curves of ρ_{ab} (Fig. 1 in Ref. [36] and Fig. 7 in Ref. [37]) do not look as good as those shown in Fig. 5.

In Fig. 5(d), we only show the experimental data for slightly underdoped La214 samples ($x = 0.1, 0.125$ and 0.14). For heavily underdoped samples ($x = 0.04, 0.06$, and 0.08), we find that the data deviate significantly from

the universal scaling curve below T^* . This deviation was observed only in the La214 samples. It may be due to the suppression of the scattering rate by the formation of stripe or other competing orders in these compounds.³⁸

In the overdoped regime, ρ_{ab} is not linear T dependent in nearly the whole temperature range.³⁹ The experimental data do not fall onto the scale curves as shown in Fig. (5). This change of the temperature behavior of ρ_{ab} in the overdoped regime can be understood from the change of the Fermi surface topology revealed by ARPES.⁴⁰ In the overdoped region the Fermi surface becomes electron-like. This may affect strongly the dynamic behavior of electrons in the CuO_2 planes.

C. The Hall coefficient $R_H(T)$

The Hall coefficient $R_H(T)$ is an important quantity in characterizing the nature of charge carriers. In a conventional metal with spheric Fermi surface and isotropic scattering rate, the Hall coefficient is inversely proportional to the carrier concentration, independent of temperature. The sign of R_H reflects the type of conducting charge carriers. R_H is negative or positive if the charge carriers are electrons or holes. However, in doped transition metal oxides, such as high- T_c cuprates, the Hall coefficient is strongly temperature dependent.^{45,46,47} It is determined not just by the carrier concentration, but also by the scattering rates and the curvature of the Fermi surface. Other effects, such as magnetic skew scattering, can also affect the temperature dependence of R_H .⁴⁸

In HTSC, R_H shows a strong temperature and doping dependence. At high temperature, R_H increases rapidly with decreasing temperature. After reaching a maximum, R_H drops down to low temperature in most of the samples. This is the typical temperature dependence of R_H in HTSC. It was observed in Y123,^{43,45} La214,^{41,44,49} Bi-systems,^{42,50,51} Hg1212⁵² and Tl-systems.^{53,54,55}

The complex temperature dependence of the Hall coefficient remains one of the hardest problems to be resolved. Within the theory of charge-spin separation, Anderson⁵⁶ proposed to use the Hall angle Θ_H instead of the Hall coefficient R_H to understand the Hall anomaly. He argued that due to the charge-spin separation, the Hall angle, which is defined by the ratio between the transverse and longitudinal conductivity, $\Theta_H = \tan^{-1} \sigma_{xy}/\sigma_{xx}$, should be determined purely by the transverse relaxation rate (i.e. the relaxation rate perpendicular to the Fermi surface). This eliminates the ambiguity in the explanation of the Hall coefficient, since it is determined by both the longitudinal and transverse relaxation rates. Anderson further argued that as the transverse relaxation rate is determined by the spin excitations which is relatively normal, the Hall angle should follow the temperature dependence of normal Fermi liquid, i.e.

$$\cot \Theta_H = \alpha T^2 + \gamma, \quad (22)$$

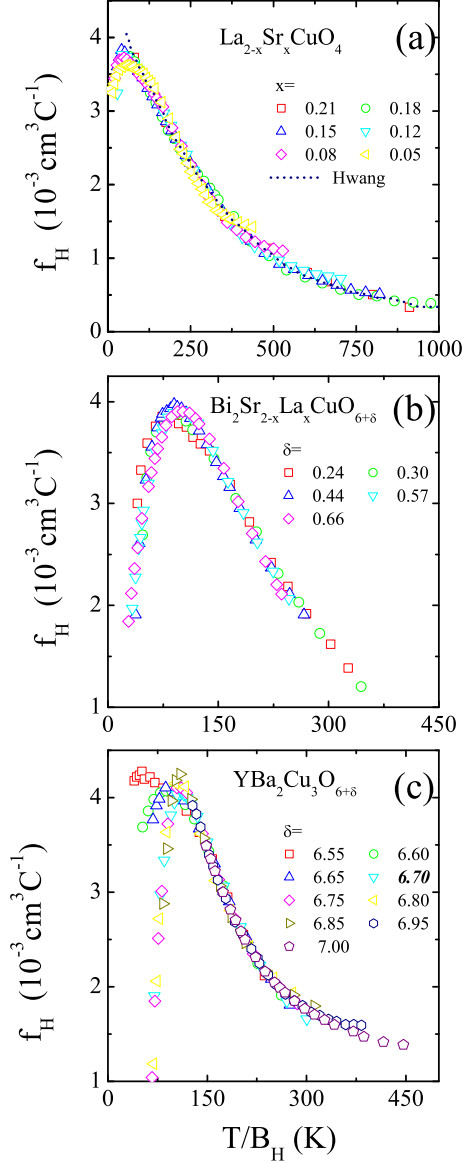


FIG. 6: The scaling functions of the Hall coefficient $R_H(T)$ for (a) La214 (Ref. [41]), (b) La-Bi2201 (Ref. [42]) and (c) Y123 (Ref. [43]). The dashed line in (a) is obtained from the scaling curves determined by Hwang et al.⁴⁴

where α is a temperature independent coefficient and γ is the impurity contribution.⁵⁷ This quadratic temperature dependence of the Hall angle indeed agrees with the experimental observation at optimal doping. However, in both under- and overdoped regimes,^{42,43,44,49,50} the temperature exponent deviates generally from 2, and the above expression breaks down.

To reveal the physics behind the anomalous temperature dependence of the Hall effect without invoking a specific model, we have analyzed the scaling behavior of

TABLE V: The scaling parameters for the Hall coefficient R_H shown in Fig. 6. The unit of C_H is $10^{-3} \text{ cm}^3 \text{ C}^{-1}$. T_c for La214 are obtained by interpolating the data given in Ref. [1]. The hole concentration p for La-Bi2201 and Y123 are obtained from Eq. (15) with the maximum $T_{c,max} = 33.03\text{K}$ for $x = 0.44$ of La-Bi2201 and 93K for $\delta = 0.95$ of Y123.

	sample	T_c (K)	doping (p)	A_H	B_H	C_H
La214	0.21	30.99	0.21	0.10	0.52	0.34
	0.18	37.14	0.18	0.25	1.08	0.23
	0.15	37.93	0.15	0.54	1.40	0.035
	0.12	31.88	0.12	0.96	1.62	-0.42
	0.08	22.3	0.08	2.23	2.15	-2.04
	0.05	2.66	0.05	4.34	2.68	-5.62
La-Bi2201	0.24	24.06	0.218	0.14	0.91	0.91
	0.3	30.0	0.194	0.22	0.87	1.11
	0.44	33.03	0.16	0.35	1.12	1.00
	0.57	28.44	0.118	0.49	1.23	1.08
	0.66	19.95	0.09	0.61	1.27	1.70
Y123	0.55	55.0	0.088	1.76	1.27	0.56
	0.6	57.0	0.091	1.52	1.15	0.20
	0.65	58	0.092	1.46	1.09	-0.035
	0.7	60.0	0.094	1.0	1.0	0.0
	0.75	62.0	0.096	0.86	1.05	-0.20
	0.8	69.0	0.103	0.67	1.08	-0.11
	0.85	83.0	0.123	0.70	0.96	-0.17
	0.95	93.0	0.16	0.35	0.78	0.073
	7.0	91.0	0.176	0.28	0.67	0.031

R_H . We assume the scaling function of R_H to have the form defined as in Eq. (10):

$$R_H(T) = A_H f_H \left(\frac{T}{B_H} \right) + C_H. \quad (23)$$

By fitting the experimental data with this formula using the method introduced in Sec. II, the scaling parameters (A_H, B_H, C_H) and the scaling function f_H can then be determined.

Fig. 6 shows the scaling function f_H for Y123, La214, and La-Bi2201. The corresponding scaling parameters are given in Table V. The experimental data were extracted from Ref. [43] for Y123, Ref. [41] for La214, and Ref. [42] for La-Bi2201. The experimental data of Y123 with $\delta < 0.55$ are not included since the temperature range measured is too narrow to allow a reliable scaling analysis to be done.

For La214, we find that R_H exhibits a good scaling behavior in nearly the whole temperature range as shown in Fig. 6(a). This is also true for La-Bi2201 Fig. 6(b). It suggests that the dynamical behavior of R_H is still governed by a single energy scale. However, in contrast to the in-plane resistivity, the scaling curve of La214 cannot be perfectly scaled onto the scaling curve of La-Bi2201, except in an intermediate temperature regime. For Y123, the experimental data can be also scaled onto a single

curve in the high temperature regime, above the peak temperature of R_H . However, in low temperatures, f_H shows very different temperature dependence for different doping. This difference might be caused by the contribution of CuO chains in Y123. Electrons in CuO chains are more disordered in the underdoped samples than in the optimally doped one.

A similar scaling analysis has been done by Hwang et al.⁴⁴ and by Chen et al.⁵⁸ The scaling equation they used is essentially the same as Eq. (23), but with different notations. In their notation, the scaling equation is given by

$$R_H(T) = R_H^\infty + R_H^* f\left(\frac{T}{T^*}\right). \quad (24)$$

R_H^∞ is the high temperature value of R_H , which is approximately temperature independent in high temperatures. T^* is a characteristic temperature to be determined. Empirically, they assumed T^* to be the crossover temperature from a temperature dependent to a temperature independent R_H at high temperature. However, the crossover temperature (if exists) is very high, well

above the temperature range they measured, in the underdoped samples. They cannot determined reliably the crossover temperature, even by extrapolation. Thus their scaling analysis cannot be applied to the underdoped samples. This is not a problem in our approach. In Fig. 6 (a), we compared the scaling curve obtained by Hwang et al.⁴⁴ with ours. We find these two scaling curves agree well with each other for La214 above the peak temperature of R_H . This suggests that the crossover temperature they determined is proportional to the parameter B_H as we determined here.

Recently, Gor'kov et al.⁵⁹ and Ono et al.⁴¹ analyzed the high temperature behavior of R_H using a two-band model in La214. They assumed the high temperature data of R_H to be thermal activated, resulting from strong charge fluctuations between the effective lower and upper Hubbard bands. They found that the high temperature data of R_H can indeed be explained by this simple picture. Their results suggests that the thermal excitation gap between the lower and upper Hubbard bands is significantly smaller than the (direct) optical charge transfer gap.

D. The thermoelectric power $S(T)$

The thermoelectric power or the Seebeck coefficient $S(T)$ is one of the transport quantities complementary to the resistivity and Hall effect. It reveals the properties of quasiparticle excitations both near and away from the Fermi level. It can be used to judge whether the charge carriers are electrons or holes from the sign of $S(T)$. It can be also used to quantify the charge carrier concentration. In HTSC, empirically, the value of $S(T)$ at $T = 290\text{K}$ was found to be a good measure of the hole concentration.⁶⁴

In high- T_c oxides, the thermopower $S(T)$ is small in the superconducting state due to the suppression of the pairing gap to the quasiparticle excitations.⁶⁴ In the normal state, $S(T)$ increases with temperature. It exhibits a maximum and then drops monotonically in high temperatures. At a given temperature, $S(T)$ decreases with increasing doping. For most of the high- T_c compounds, including Bi2212,^{64,65,66,67} La-Bi2201,^{68,69} Tl1212,^{64,65} and Hg1201,^{62,70,71} $S(T)$ is positive in the underdoped regime, but becomes negative in the overdoped regime. At optimal doping, $S(T)$ becomes negative at high temperature. However, in La214, $S(T)$ was found to be positive in the whole doping range.^{60,63,72} The thermopower of overdoped Y-based cuprates also behaves differently from other compounds. It shows a positive slope, in contrast to the negative slope in other compounds, at high temperature. This is probably due to the contribution of

CuO chains.

We have applied our scaling approach to the thermoelectric power. The scaling formula is given by

$$S(T) = A_S f_S\left(\frac{T}{B_S}\right) + C_S. \quad (25)$$

Fig. 7 shows the scaling curves for Y123, Ca-Y123, Hg1201 and La214. The scaling parameters are listed in Tables VI and VII. The experimental data were extracted from Ref. [60] for Y123, Ref. [61] for Ca-Y123, Ref. [62] for Hg1201 and Refs. [60,63] for La214. The scaling curves for two heavily underdoped samples with $T_c < 2\text{K}$ and three heavily overdoped samples of Hg1201 (Ref.[62]) deviate significantly from the universal scaling curve and are not included in the figure. For Y123 and Ca-Y123 we only analyze the underdoped samples since in the overdoped regime the chain contribution becomes important, which breaks the scaling law. The chain contribution can in fact be seen already in the slightly underdoped sample of Y123 ($\delta = 0.175$), whose high temperature data of $S(T)$ already begin to deviate away from the scaling curve in high temperatures. For some samples of Hg1201 and Ca-Y123, the measurement data fall faster than the universal scaling curves in low temperatures. This can be attributed to the superconducting fluctuations.

The scaling behavior of $S(T)$ in HTSC has been extensively studied by a number of groups using the scaling formula like that as defined in Eq. (14).^{60,62,65,67,71} Our

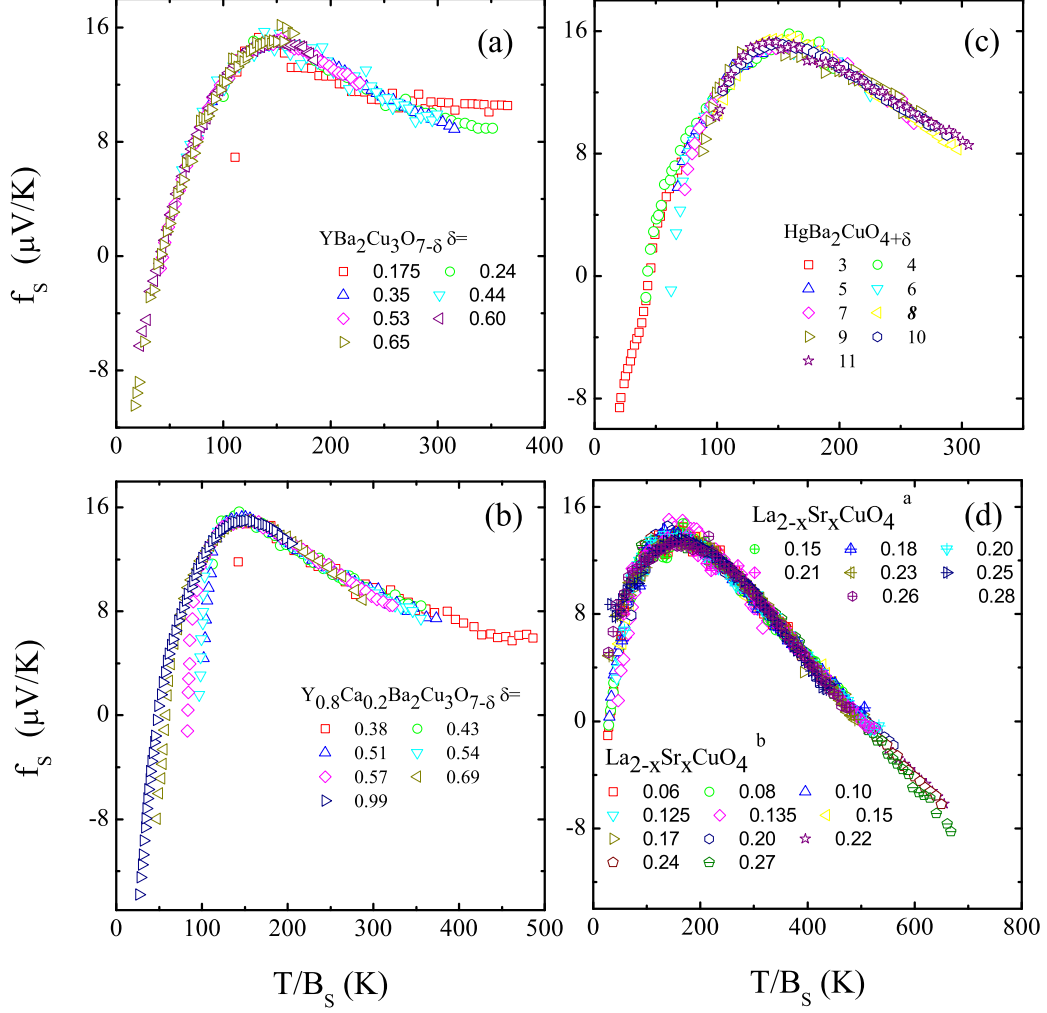


FIG. 7: The scaling function of the thermoelectric power $S(T)$ for Y123 (Ref. [60]), Ca-Y123 (Ref. [61]), Hg1201 (Ref. [62]), La214^a (Ref. [63]) and La214^b (Ref. [60]). The notations defined in Ref. [62] are used to label the Hg1201 samples. Sample 8 of Hg1201 is the reference one.

scaling curves are consistent with their results. However, our data are much less scattered than theirs.

E. The uniform magnetic susceptibility $\chi(T)$

The uniform magnetic susceptibility $\chi(T)$ measures basically the density of states at the Fermi level in conventional Landau Fermi liquid. However, in high- T_c copper oxides, the susceptibility is strongly affected by antiferromagnetic spin fluctuations. The parent compounds of HTSC are half-filled antiferromagnetic Mott insulators with long-range Néel order.⁷³ Upon doping, the Néel or-

der is rapidly suppressed, but antiferromagnetic fluctuations persist up to slightly overdoping.^{74,75}

At half-filling, $\chi(T)$ shows a sharp peak around the Néel temperature.^{76,77} This peak shifts down to lower temperature with doping and disappears completely when the superconductivity emerges. In the normal state, the magnetic susceptibility $\chi(T)$ first increases with increasing temperature, develops a broad peak, and then drops down at high temperature.^{18,30,78,79,80,81,82}

In real materials, the magnetic susceptibility is strongly affected by magnetic impurities. These impurities contribute a Curie term to χ , which diverges as $1/T$ in low temperatures. The impurity contribution is

TABLE VI: The scaling parameters for the thermoelectric power $S(T)$ of Y123, Ca-Y123 and Hg1201 in Fig. 7. The unit of C_S is $\mu\text{V/K}$. Sample 8 of Hg1201 is taken as a reference.

	sample	T_c (K)	doping (p)	A_S	B_S	C_S
Y123	0.65			75.53	1.80	4.17
	0.60	13.31	0.057	60.37	1.60	3.22
	0.53	44.66	0.079	42.42	1.27	2.46
	0.44	55.51	0.089	15.67	0.99	2.36
	0.35	59.8	0.093	10.36	0.94	2.03
	0.24	74.4	0.109	1.18	0.83	1.46
Ca-Y123	0.175	90.7	0.14	-1.46	0.79	0.48
	0.38	85.50	0.16	0.31	0.61	-1.17
	0.43	85.00	0.151	0.41	0.80	-1.07
	0.51	81.58	0.136	0.99	0.81	-1.57
	0.54	78.55	0.128	1.10	0.84	1.13
	0.57	77.19	0.125	1.15	0.85	4.21
Hg1201:	0.69	47.04	0.085	1.46	1.05	12.86
	0.99	37.69	0.077	2.01	1.40	30.07
	3	26.0	0.05	3.65	1.58	33.56
	4	46.0	0.057	3.81	1.43	11.79
	5	62.0	0.069	2.50	1.33	15.24
	6	72.0	0.09	1.98	1.26	4.88
	7	77.0	0.103	1.90	1.12	-3.27
	8	83.0	0.11	1.0	1.0	0.0
	9	91.0	0.119	1.18	1.07	-4.67
	10	95.0	0.127	0.96	1.01	-2.80
	11	98.0	0.157	0.68	0.98	-3.01

strongly sample dependent. In order to analyze the intrinsic behavior of the magnetic susceptibility, this Curie term of impurities should be subtracted from the raw data first.

To elucidate the intrinsic property of the magnetic susceptibility, we have analyzed the scaling behavior of $\chi(T)$ with the following single-parameter scaling equation

$$\chi(T) = A_\chi f_\chi \left(\frac{T}{B_\chi} \right) + C_\chi. \quad (26)$$

Fig. 8 shows the scaling curves of $\chi(T)$ for La214 and Bi2212. The experimental data were extracted from those published by Nakano et al.³⁰ for La214 and by Watanabe et al.¹⁸ for Bi2212. The corresponding scaling parameters are shown in Table VIII. In the scaling analysis for the La214 samples with $x = 0.20, 0.22$ and 0.26 , a Curie-term C/T is subtracted from the experimental data, the corresponding values of C , i.e., $C = 12.41, 37.23$ and 60.23 (in units of 10^{-7} emu/g) were obtained by Nakano et al.³⁰

We find that the susceptibility for both La214 and Bi2212 exhibits a good scaling behavior. For Bi2212, $\chi(T)$ in heavily overdoped samples begins to deviate from the scaling curve near T_c . This is likely to be due to strong superconducting fluctuations.

TABLE VII: The scaling parameters for the thermoelectric power $S(T)$ of La214 in Fig. 7. The data are referenced to Sample 8 of Hg1201 shown in Table VI. The unit of C_S is $\mu\text{V/K}$. T_c of La214^a is obtained from the data published in Ref. [1] by interpolation. T_c of La214^b is obtained from Fig. 1 of Ref. [60].

	sample	T_c (K)	doping (p)	A_S	B_S	C_S
La214 ^a	0.15	37.93	0.15	1.23	0.87	16.44
	0.18	37.14	0.18	0.90	0.69	8.07
	0.2	34.62	0.2	0.74	0.63	5.70
	0.21	30.99	0.21	0.64	0.60	4.46
	0.23	23.77	0.23	0.52	0.61	1.95
	0.25	17.29	0.25	0.45	0.65	0.15
	0.26	14.4	0.26	0.42	0.72	-1.48
	0.28	8.08	0.28	0.44	0.67	-0.85
	0.06	5.0	0.06	53.51	2.01	4.18
	0.08	22.3	0.08	51.78	1.74	3.22
La214 ^b	0.1	30.75	0.1	40.03	1.54	2.53
	0.125	32.0	0.125	31.55	1.17	1.66
	0.135	35.9	0.135	30.04	1.01	0.88
	0.15	37.93	0.15	18.66	0.78	0.79
	0.17	38.4	0.17	17.73	0.69	0.87
	0.2	34.62	0.2	10.59	0.62	0.83
	0.22	27.81	0.22	6.34	0.54	0.61
	0.24	19.96	0.24	3.41	0.54	0.53
	0.27	12.0	0.27	2.69	0.53	0.43

Our universal scaling curve is consistent with the scaling analysis given by Johnston et al.⁸⁰ and Nakano et al.³⁰ for La214, and Allgeier et al.⁸² for Bi2212. The scaling analysis of Nakano et al. was made based on the scaling formula defined by Eq. (14).³⁰ The problem with that kind of analysis is that the characteristic temperature T^* defined in Eq. (14) has to be determined empirically prior to the scaling analysis. The characteristic temperature T^* for the susceptibility was generally determined from the peak temperature of χ . However, in heavily overdoped samples, no peak structure has been observed within the whole temperature measured. This has limited the application of that kind of scaling analysis. In addition, to fully satisfy Eq. (14), a constant term needs also be subtracted for each set of data. This is also difficult if the measured temperature range is not broad enough. Nevertheless, we find that their scaling curves, as shown in Fig. (8), agree well with ours.

The scaling analysis given by Johnston et al.⁸⁰ and Allgeier et al.⁸² are based on the high-temperature series expansion for 2D antiferromagnetic Heisenberg model. The scaling function obtained by Johnston et al. deviates slightly from the universal scaling curve obtained at high temperature. The high temperature scaling curve, as shown by Johnston et al.⁸⁰ and Allgeier et al.⁸², agrees with the temperature dependence of the susceptibility of the two-dimensional antiferromagnetic Heisenberg model

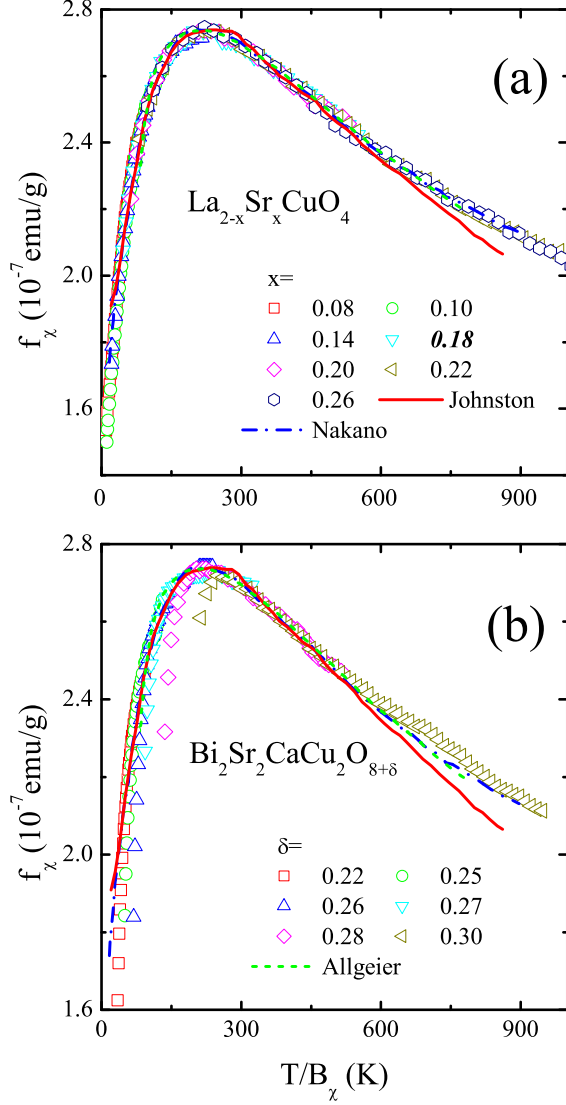


FIG. 8: The scaling function of the uniform magnetic susceptibility $\chi(T)$ for La214 (Ref. [30]) and Bi2212 (Ref. [18]). The solid, dash-dot and dash lines represent the rescaled scaling curves obtained by Johnston (Ref. [80]), Nakano et al (Ref. [30]) and Allgeier et al. (Ref. [82]), respectively.

without doping.

In obtaining the scaling function, a temperature independent term is subtracted from $\chi(T)$. This term can be expressed as

$$\chi_0 = C_\chi + A_\chi \chi_{0,s}, \quad (27)$$

where $\chi_{0,s}$ is the value of χ_0 for the reference sample. The variation of χ_0 with doping may reflect the change of the density of states at the Fermi level. Thus it is interesting to analyze the doping dependence of this term.

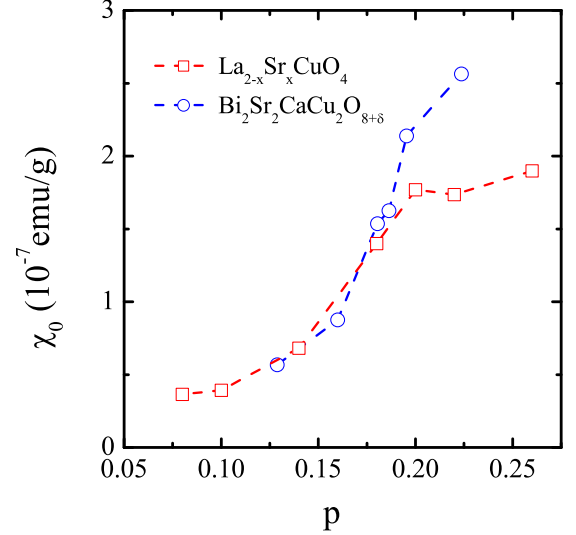


FIG. 9: The temperature independent magnetic susceptibility $\chi_0 = C_\chi + A_\chi \chi_{0,s}$ where $\chi_{0,s} = 1.4 \times 10^{-7}$ emu/g for La214 with $x = 0.18$ as obtained from Nakano et al.³⁰

Fig. 9 shows the doping dependence of χ_0 . χ_0 increases monotonically with doping. This temperature independent term might be the contribution of the core diamagnetism, the Van Vleck paramagnetism, the Landau diamagnetism, and the Pauli paramagnetism of the band electrons if the effect of antiferromagnetic correlations is ignored. The core diamagnetism and the Van Vleck paramagnetism are doping independent. The Landau diamagnetism is generally small. Thus the doping dependence of χ_0 is mainly affected by the Pauli susceptibility, which is proportional to the density of states at the Fermi level. Hence the change of χ_0 with doping will correspond to the change of the density of states at the Fermi level. This simple observation is consistent with the result of Allgeier et al.⁸² as well as the measurement of the specific heat.¹

F. The spin-lattice relaxation rate $1/T_1$

The nuclear magnetic resonance (NMR) probes the local spin dynamics via the measurement of the Knight shift, the spin-lattice relaxation rate $1/T_1$, and other spin response functions.⁸³ The Knight shift measures the shift of the resonance frequency induced by the conduction electrons. It is proportional to the uniform magnetic susceptibility $\chi(T)$. The temperature dependence of the Knight shift should follow the scaling law of the uniform susceptibility as discussed in the previous section. This is indeed supported by the experimental measurement (see, for example, Ref. [84]). Below we will discuss the scaling

TABLE VIII: The scaling parameters for the magnetic susceptibility $\chi(T)$ shown in Fig. (8). The unit of C_χ is 10^{-7} emu/g. T_c of La214 is obtained from Ref. [1] by interpolation. In obtaining the scaling curves, a Curie-term C/T is subtracted from the measurement data for the La214 samples with $x = 0.20, 0.22$ and 0.26 . The corresponding values of C , obtained from Fig. 8 of the Ref. [30], are 12.41, 37.23 and 60.23×10^{-7} emu/g, respectively.

	sample	T_c (K)	doping (p)	A_χ	B_χ	C_χ
La214	0.08	22.3	0.08	1.40	5.97	-1.60
	0.10	30.75	0.10	1.41	4.18	-1.57
	0.14	36.62	0.14	1.28	2.31	-1.11
	0.18	37.45	0.18	1.0	1.0	0.0
	0.20	34.62	0.20	1.04	0.68	0.31
	0.22	27.81	0.22	1.24	0.53	-0.001
	0.26	14.57	0.26	1.38	0.46	-0.027
Bi2212	0.22	82.0	0.13	1.33	3.04	-1.29
	0.25	89.57	0.16	1.10	2.22	-0.66
	0.26	87.19	0.18	0.66	1.60	0.61
	0.27	83.45	0.186	0.72	1.18	0.62
	0.28	78.7	0.195	0.51	0.74	1.42
	0.30	68.51	0.22	0.66	0.40	1.84

behavior of the spin-lattice relaxation rate $1/T_1$.

The high temperature dependence of $1/T_1T$ of ^{63}Cu shows a Curie-Weiss-like behavior.^{85,86} This can be attributed to the contribution of antiferromagnetic fluctuations since $1/T_1T$ of ^{63}Cu is dominated by spin fluctuations near $Q = (\pi, \pi)$. It exhibits a broad maximum in an intermediate temperature regime and then drops in low temperature.

TABLE IX: The fitting parameters, A_{T_1} , B_{T_1} , and C_{T_1} for the scaling analysis of $1/T_1T$ shown in Fig. 10. The unit of C_{T_1} for ^{63}Cu of Bi2212 and Tl1212 is $\text{sec}^{-1}\text{K}^{-1}$ and for ^{89}Y of Y123 is $10^{-4}\text{sec}^{-1}\text{K}^{-1}$.

	sample	T_c (K)	doping (p)	A_{T_1}	B_{T_1}	C_{T_1}
Bi2212 ^{63}Cu	0.125	79.0	0.13	0.86	1.31	0.72
	0.20	86.0	0.16	1.0	1.0	0.0
	0.225	77.3	0.20	1.17	0.85	-1.67
Tl1212 ^{63}Cu		70.0		2.44	0.72	-4.72
		54.0		2.29	0.56	-3.05
		10.0		0.48	0.16	16.18
Y123 ^{89}Y	1.0	88.8	0.19	0.075	0.88	1.51
	1- ϵ			0.069	1.35	1.53
	0.85	90.3	0.14	0.085	1.63	1.15
	0.75	67.9	0.10	0.087	1.50	0.83
	0.63	57.3	0.09	0.088	2.30	0.90
	0.53	52.5	0.086	0.097	2.80	0.80
	0.48	38.0	0.07	0.070	3.35	0.77
	0.41	15.0	0.06	0.028	3.74	0.68

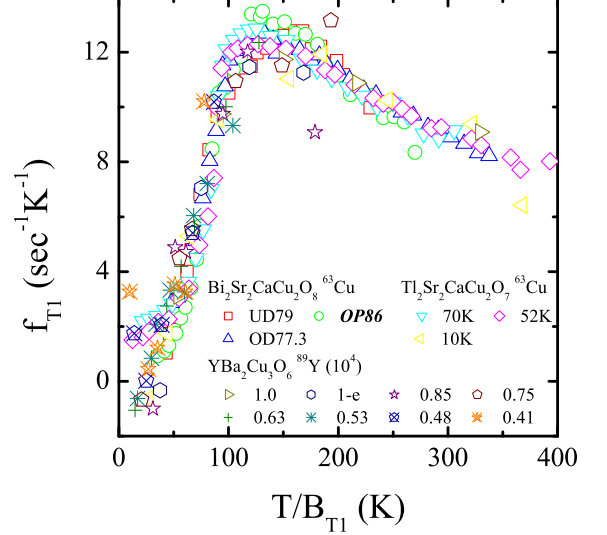


FIG. 10: The scaling function for $1/T_1T$ of ^{63}Cu in Bi2212 and Tl1212, and that of ^{89}Y in Y123. The experimental data are obtained from Ref. [87] for Bi2212, Ref. [86] for Tl1212, and Ref. [88] for Y123. The notations of the samples are the same as those in the corresponding references. The Bi2212 OP86 is taken as the reference sample.

We have analyzed the scaling behavior of the experimental data of $1/T_1T$ published by Ishida et al.⁸⁷ for ^{63}Cu in Bi2212, by Magishi et al.⁸⁶ for ^{63}Cu in Tl1212, and by Alloul et al.⁸⁸ for ^{89}Y in Y123. The scaling equation is assumed to be

$$\frac{1}{T_1T} = A_{T_1}f_{T_1}\left(\frac{T}{B_{T_1}}\right) + C_{T_1}. \quad (28)$$

Fig. 10 shows the temperature dependence of the scaling function f_{T_1} . The corresponding scaling parameters are given in Table. IX.

Within experimental errors, we find that $1/T_1T$ shows a good scaling behavior. For all the materials shown in Fig. (10), the data of $1/T_1T$ can be scaled on a common curve in a relatively wide range of temperature. This, again, suggests that the normal state dynamics is controlled by a single energy scale. This single-parameter scaling behavior is consistent with the existing theory of spin fluctuations, such as the antiferromagnetic Fermi liquid theory proposed by Millis et al.⁸⁹

IV. ANALYSIS OF THE CHARACTERISTIC ENERGY SCALE

In the preceding section, we have analyzed the scaling behaviors of the transport coefficients, including the

resistivity, the Hall effect and the thermoelectric power, and the magnetic response functions, including the spin susceptibility and the spin-lattice relaxation rate, in the normal state of HTSC. These coefficients probe different aspects of low energy excitations and are physically distinct. However, we find that they all show good scaling behaviors. For most of the measurement quantities, the temperature dependence of the corresponding scaling functions are universal, depending neither on the doping concentration nor on the chemical structure of the materials measured.

Among the three scaling parameters, the energy scale Δ or the relative energy scale B defined in Eq. (7), is the most important one. It characterizes the basic energy scale governing the temperature dependence of a response function. For the c-axis resistivity, we have determined the absolute values of Δ using the approximate scaling function of ρ_c derived in our previous work for multilayer cuprates.⁶ For other measurement quantities, as the analytic formula of the scaling functions are unknown, only the ratio of Δ with respect to a reference sample, $B = \Delta/\Delta_s$, are determined. Nevertheless, we find that these characteristic energy parameters determined from different coefficients show a common trend with doping. As shown in Tables III-VII, they all decrease with increasing doping.

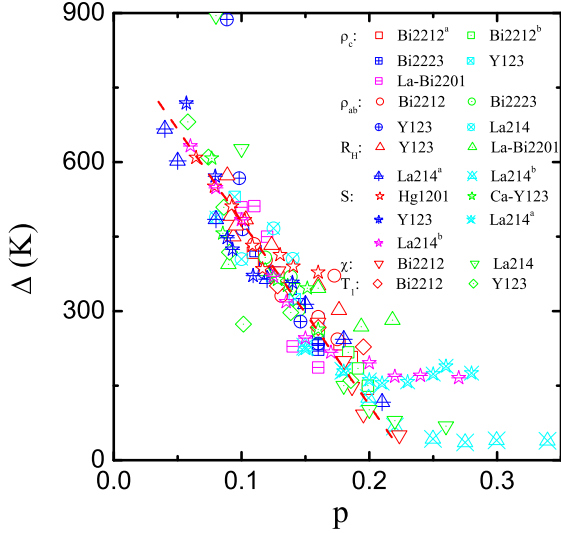


FIG. 11: The doping dependence of the energy scales obtained with Eq. (29). The values of the scaling factor η_y are listed in Table X. The dashed line is the linear fit to the scaled pseudogap energies obtained by various experimental probes. Here we take the pseudogap energy obtained from the c-axis resistivity of Bi2212 as a reference, as shown in Fig. 3.

The similar doping dependence of the characteristic energy parameters suggests that these relative energy scales obtained by different probes may have a common phys-

TABLE X: The values of the scaling factor η_y for different probes $y = \rho_c, \rho_{ab}, R_H, \chi, 1/T_1T$, and S of the cuprates. The superscripts a and b for S and R_H of La214 refer to the data published in Ref. [41] and Ref. [44], respectively.

	ρ_c	ρ_{ab}	R_H	S	χ	T_1T
Bi2212	1	455	-	-	125	267
Bi2223	1.04	375	-	-	-	-
Y123	1.67	465	450	450	-	182
Ca-Y123	-	-	-	435	-	-
La214	-	405	225 ^a	255 ^a	150	-
	-	-	0.46 ^b	315 ^b	-	-
La-Bi2201	450	-	310	-	-	-
Hg1201	-	-	-	385	-	-

ical origin. This can be examined by rescaling all the relative energy scales with respect to the absolute energy scale of the pseudogap Δ obtained from the scaling analysis of ρ_c . They should fall onto a single curve if they are indeed the pseudogap energies. To do this, let us introduce the following formula

$$\Delta_y(p) = \eta_y B_y(p), \quad (29)$$

where η_y is a scaling factor and Δ_y is the characteristic energy scale. The subscript y represents the measured physical quantity, i.e. $y = \rho_c, \rho_{ab}, R_H, S, \chi$, and $1/T_1T$. The scaling factors η_y can be determined by the least square fit, using the approach introduced in Sec. II.

The fitting parameters of η_y are given in Table X. By substituting them into Eq. (29), we can obtain the values of Δ_y . The result, as shown in Fig. 11, indicates that all the energy scales determined from the scaling analysis given in Sec. III have the same doping dependence within experimental errors, which result mainly from the uncertainty in the determination of doping concentration. It suggests that all the dynamic coefficients analyzed in Sec. III are indeed governed by the same energy scale. This is a remarkable result since different coefficients probe different responses of charge and/or spin degrees of freedom. For example, the c-axis resistivity ρ_c is susceptible to the charged excitations around the antinodal points, while the in-plane resistivity ρ_{ab} is mainly affected by the scattering of charged quasiparticles around the node points. The uniform magnetic susceptibility probes the spin fluctuations around $\mathbf{k} = (0, 0)$, while the spin-lattice relaxation rate is strongly dependent on the antiferromagnetic fluctuations around $\mathbf{k} = (\pi, \pi)$.

In the underdoped regime, the characteristic energy Δ drops almost linearly with doping. This is consistent with the doping dependence of the pseudogap observed by ARPES,⁹⁰ tunnelling,⁹¹ as well as other measurement.²⁵ Thus the control energy scale in this regime is indeed the pseudogap. If we extrapolate the underdoped data of Δ to zero doping, we find that Δ is in order of J , and to higher doping, Δ vanishes roughly at $p \sim 0.23-0.25$.

In the literature, two kinds of pseudogaps (or the onset temperatures of pseudogap), which were often quoted as the "large" and "small" pseudogaps, were reported.⁴ The large pseudogap generally refers to the characteristic temperature T^* measured, for example, by the magnetic susceptibility,³⁰ the Hall coefficient.⁴⁴ The small one could be the energy scale probed by other experimental techniques, such as the transport properties measurements³¹ or the leading-edge shift around the antinodal direction measured by the ARPES.⁹² Our scaling analysis indicates that these two energy scales are in fact physically indistinguishable.

In the overdoped regime, the universal scaling behavior generally breaks down. For overdoped La214, Δ_y determined from the thermopower and the Hall coefficients separates into two branches with different energies. Δ_y determined from the thermopower is higher than that from the Hall effect. This may imply the existence of two energy scales in the overdoped regime. However, as the single parameter scaling law still holds in this regime for both the thermopower and the Hall coefficients, further investigation on this issue is desired.

Recently, there is a surge of interests in the discussion of two gap energies, namely the pseudogap in the normal state and the relatively smaller superconducting gap in the superconducting state. The existence of a distinct energy scale in the superconducting state, whose doping dependence is different to that of the pseudogap, was first reported in the Andreev reflection measurements⁹³ and more systematically in the penetration depth measurements.⁹⁴ This lower energy scale characterizes the low-lying excitations around the gap nodes and appears only in the superconducting state. Recently, both the Raman scattering and the ARPES have further confirmed the existence of these two distinguished energy scales.^{25,95} Furthermore, the ARPES has revealed that the two-gap structure is intimately connected with the arc (or pocket) feature of the Fermi surface of HTSC in the underdoped regime. It is believed that the superconducting gap develops predominately on the Fermi arc below T_c . However, there exists also other experimental measurements, which suggest that there is only one energy scale in the superconducting state and the superconducting gap around the nodal points is nothing but an extension of the pseudogap in the arc area in the

superconducting state.⁹⁶ This one energy scale scenario is consistent with the picture of resonant valence bonds based on the charge-spin separation⁹⁷ as well as that of preformed pairs.⁹⁸

In this work, we have shown that there is only one energy scale in the normal state. However, as we have only analyzed the scaling behavior of the experimental data in the normal state, we are unable to address the issue of two energy gaps in the superconducting state. It is of great interest to extend the single-parameter scaling method introduced in Sec. II to the superconducting state at which two energy scales (or control parameters) may exist. This would then allow us to judge whether there is only one or two energy scales in the superconducting state from the model-independent scaling analysis of various transport and thermodynamic coefficients.

V. SUMMARY

We have introduced a novel scaling method to study the scaling behavior in the normal state of HTSC. We have analyzed the scaling behavior of the c-axis resistivity, the in-plane resistivity, the Hall coefficient, the thermoelectric power, the magnetic susceptibility and the nuclear magnetic resonance, and extracted the corresponding energy scales. It is found that all these quantities, no matter how different they are, exhibit universal scaling behaviors, controlled by a single energy scale in the normal state. Furthermore, we find that all these energy scales obtained from different physical coefficients have the same doping dependence as the pseudogap. It shows that the pseudogap is the only characteristic energy governing the low-lying excitations in the normal state of HTSC.

The scaling method we introduced in Sec. II is model independent. It provides a simple but powerful tool to analyze the scaling behavior of experimental data. It can be applied not only to the normal state of HTSC, but also to any other systems where the single-parameter scaling hypothesis, i.e. Eq. (3) or (10), is valid.

Acknowledgement Support from the NSFC and the national program for basic research of China is acknowledged.

¹ J. W. Loram, K. A. Mirza, and J. R. Cooper, P77 in *High Temperature Superconductivity*, edited by W. Y. Liang (Cambridge Marketing Limited, 1998).

² C. Panagopoulos, J. L. Tallon, B. D. Rainford, T. Xiang, J. R. Cooper, and C. A. Scott, Phys. Rev. B **66**, 064501 (2002).

³ S. H. Pan, E. W. Hudson, K. M. Lang, H. Eisaki, S. Uchida, and J. C. Davis, Nature **403**, 746 (2000).

⁴ T. Timusk and B. Statt, Rep. Prog. Phys. **62**, 61 (1999).

⁵ C. M. Varma, P. B. Littlewood, S. Schmitt-Rink, E. Abra-

hams, and A. E. Ruckenstein, Phys. Rev. Lett. **63**, 1996 (1989).

⁶ Y. H. Su, H. G. Luo, and T. Xiang, Phys. Rev. B **73**, 134510 (pages 6) (2006).

⁷ T. Xiang and J. M. Wheatley, Phys. Rev. Lett. **77**, 4632 (1996).

⁸ T. Xiang, C. Panagopoulos, and J. R. Cooper, Int. J. Mod. Phys. B **12**, 1007 (1998).

⁹ See, e.g., William H. Press, Saul A. Teukolsky, William T. Vetterling, Brian P. Flannery, *Numerical Recipes in C, The*

- Art of Scientific Computing* (Cambridge University Press, 1992).
- ¹⁰ T. Ito, K. Takenaka, and S. Uchida, Phys. Rev. Lett. **70**, 3995 (1993).
 - ¹¹ M. Presland, J. Tallon, R. Buckley, R. Liu, and N. Flower, Physica C **176**, 1324 (1991).
 - ¹² P. W. Anderson and Z. Zou, Phys. Rev. Lett. **60**, 132 (1988).
 - ¹³ N. Kumar and A. M. Jayannavar, Phys. Rev. B **45**, 5001 (1992).
 - ¹⁴ N. Nagaosa, Phys. Rev. B **52**, 10561 (1995).
 - ¹⁵ M. Turlakov and A. J. Leggett, Phys. Rev. B **63**, 064518 (2001).
 - ¹⁶ P. B. Littlewood and C. M. Varma, Phys. Rev. B **45**, 12636 (1992).
 - ¹⁷ T. Watanabe, T. Fujii, and A. Matsuda, Phys. Rev. Lett. **79**, 2113 (1997).
 - ¹⁸ T. Watanabe, T. Fujii, and A. Matsuda, Phys. Rev. Lett. **84**, 5848 (2000).
 - ¹⁹ The experimental data of $\delta = 0.28$ in Bi2212 is from T. Watanabe.
 - ²⁰ T. Fujii, I. Terasaki, T. Watanabe, and A. Matsuda, Phys. Rev. B **66**, 024507 (2002).
 - ²¹ Y. F. Yan, P. Matl, J. M. Harris, and N. P. Ong, Phys. Rev. B **52**, R751 (1995).
 - ²² D. Babić, J. R. Cooper, J. W. Hodby, and C. Chen, Phys. Rev. B **60**, 698 (1999).
 - ²³ M. Giura, R. Fastampa, S. Sarti, and E. Silva, Phys. Rev. B **68**, 134505 (2003).
 - ²⁴ N. Miyakawa, P. Guptasarma, J. F. Zasadzinski, D. G. Hinks, and K. E. Gray, Phys. Rev. Lett. **80**, 157 (1998).
 - ²⁵ M. L. Tacon, A. Sacuto, A. Georges, G. Kotliar, Y. Gallais, D. Colson, and A. Forget, Nature Physics **2**, 537 (2006).
 - ²⁶ X. H. Chen, M. Yu, K. Q. Ruan, S. Y. Li, Z. Gui, G. C. Zhang, and L. Z. Cao, Phys. Rev. B **58**, 14219 (1998).
 - ²⁷ S. Ono and Y. Ando, Phys. Rev. B **67**, 104512 (2003).
 - ²⁸ Y. Ando, G. S. Boebinger, A. Passner, T. Kimura, and K. Kishio, Phys. Rev. Lett. **75**, 4662 (1995).
 - ²⁹ Y. Ando, S. Komiya, K. Segawa, S. Ono, and Y. Kurita, Phys. Rev. Lett. **93**, 267001 (pages 4) (2004).
 - ³⁰ T. Nakano, M. Oda, C. Manabe, N. Momono, Y. Miura, and M. Ido, Phys. Rev. B **49**, 16000 (1994).
 - ³¹ B. Batlogg, H. Y. Hwang, H. Takagi, R. J. Cava, H. L. Kao, and J. Kwo, Physica C **235-240**, 130 (1994).
 - ³² S. Martin, A. T. Fiory, R. M. Fleming, L. F. Schneemeyer, and J. V. Waszczak, Phys. Rev. B **41**, 846 (1990).
 - ³³ N. Nagaosa and P. A. Lee, Phys. Rev. Lett. **64**, 2450 (1990).
 - ³⁴ L. B. Ioffe and P. B. Wiegmann, Phys. Rev. Lett. **65**, 653 (1990).
 - ³⁵ T. Moriya, Y. Takahashi, and K. Ueda, J. Phys. Soc. Jpn. **59**, 2905 (1990).
 - ³⁶ B. Wuyts, V. V. Moshchalkov, and Y. Bruynseraede, Phys. Rev. B **51**, 6115 (1995).
 - ³⁷ B. Wuyts, V. V. Moshchalkov, and Y. Bruynseraede, Phys. Rev. B **53**, 9418 (1996).
 - ³⁸ J. M. Tranquada, B. J. Sternlieb, J. D. Axe, Y. Nakamura, and S. Uchida, Nature **375**, 561 (1995).
 - ³⁹ H. Takagi, B. Batlogg, H. L. Kao, J. Kwo, R. J. Cava, J. J. Krajewski, and W. F. Peck, Phys. Rev. Lett. **69**, 2975 (1992).
 - ⁴⁰ A. Ino, C. Kim, M. Nakamura, T. Yoshida, T. Mizokawa, A. Fujimori, Z.-X. Shen, T. Kakeshita, H. Eisaki, and S. Uchida, Phys. Rev. B **65**, 094504 (2002).
 - ⁴¹ S. Ono, S. Komiya, and Y. Ando, Phys. Rev. B **75**, 024515 (pages 8) (2007).
 - ⁴² Y. Ando and T. Murayama, Phys. Rev. B **60**, R6991 (1999).
 - ⁴³ K. Segawa and Y. Ando, Phys. Rev. B **69**, 104521 (pages 8) (2004).
 - ⁴⁴ H. Y. Hwang, B. Batlogg, H. Takagi, H. L. Kao, J. Kwo, R. J. Cava, J. J. Krajewski, and W. F. Peck, Phys. Rev. Lett. **72**, 2636 (1994).
 - ⁴⁵ T. R. Chien, Z. Z. Wang, and N. P. Ong, Phys. Rev. Lett. **67**, 2088 (1991).
 - ⁴⁶ L. Forro, D. Mandrus, C. Kendziora, L. Mihaly, and R. Reeder, Phys. Rev. B **42**, 8704 (1990).
 - ⁴⁷ W. Jiang, J. L. Peng, S. J. Hagen, and R. L. Greene, Phys. Rev. B **46**, 8694 (1992).
 - ⁴⁸ A. T. Fiory and G. S. Grader, Phys. Rev. B **38**, 9198 (1988).
 - ⁴⁹ Y. Ando, Y. Kurita, S. Komiya, S. Ono, and K. Segawa, Phys. Rev. Lett. **92**, 197001 (pages 4) (2004).
 - ⁵⁰ Z. Konstantinović, Z. Z. Li, and H. Raffy, Phys. Rev. B **62**, R11989 (2000).
 - ⁵¹ L. Fruchter, H. Raffy, F. Bouquet, and Z. Z. Li, Phys. Rev. B **75**, 092502 (pages 4) (2007).
 - ⁵² J. M. Harris, H. Wu, N. P. Ong, R. L. Meng, and C. W. Chu, Phys. Rev. B **50**, 3246 (1994).
 - ⁵³ P. S. Wang, J. C. Williams, K. D. D. Rathnayaka, B. D. Hennings, D. G. Naugle, and A. B. Kaiser, Phys. Rev. B **47**, 1119 (1993).
 - ⁵⁴ T. Manako and Y. Kubo, Phys. Rev. B **50**, 6402 (1994).
 - ⁵⁵ Y. Shimakawa, J. D. Jorgensen, T. Manako, and Y. Kubo, Phys. Rev. B **50**, 16033 (1994).
 - ⁵⁶ P. W. Anderson, Phys. Rev. Lett. **67**, 2092 (1991).
 - ⁵⁷ G. Xiao, P. Xiong, and M. Z. Cieplak, Phys. Rev. B **46**, 8687 (1992).
 - ⁵⁸ N. Y. Chen, V. C. Matijasevic, J. E. Mooij, and D. van der Marel, Phys. Rev. B **50**, 16125 (1994).
 - ⁵⁹ L. P. Gor'kov and G. B. Teitelbaum, Phys. Rev. Lett. **97**, 247003 (pages 4) (2006).
 - ⁶⁰ J. R. Cooper and J. W. Loram, J. Phys. I France **6**, 2237 (1996).
 - ⁶¹ C. Bernhard and J. L. Tallon, Phys. Rev. B **54**, 10201 (1996).
 - ⁶² A. Yamamoto, W.-Z. Hu, and S. Tajima, Phys. Rev. B **63**, 024504 (2000).
 - ⁶³ J.-S. Zhou and J. B. Goodenough, Phys. Rev. B **51**, 3104 (1995).
 - ⁶⁴ S. D. Obertelli, J. R. Cooper, and J. L. Tallon, Phys. Rev. B **46**, 14928 (1992).
 - ⁶⁵ A. N. D. J B Mandal and B. Ghosh, J. Phys.: Condens. Matter **8**, 3047 (1996).
 - ⁶⁶ M. Akoshima, T. Noji, Y. Ono, and Y. Koike, Phys. Rev. B **57**, 7491 (1998).
 - ⁶⁷ T. S. T Takemura, T Kitajima and I. Terasaki, Journal of Physics: Condensed Matter **12**, 6199 (2000).
 - ⁶⁸ Y. Dumont, C. Ayache, and G. Collin, Phys. Rev. B **62**, 622 (2000).
 - ⁶⁹ Z. Konstantinović, G. Le Bras, A. Forget, D. Colson, F. Jean, G. Collin, M. Ocio, and C. Ayache, Phys. Rev. B **66**, 020503 (2002).
 - ⁷⁰ A. Yamamoto, K. Minami, W.-Z. Hu, A. Miyakita, M. Izumi, and S. Tajima, Phys. Rev. B **65**, 104505 (2002).
 - ⁷¹ T. Honma, P. H. Hor, H. H. Hsieh, and M. Tanimoto, Phys. Rev. B **70**, 214517 (pages 10) (2004).
 - ⁷² N. Kakinuma, Y. Ono, and Y. Koike, Phys. Rev. B **59**,

- 1491 (1999).
- ⁷³ D. Vaknin, S. K. Sinha, D. E. Moncton, D. C. Johnston, J. M. Newsam, C. R. Safinya, and H. E. King, *Phys. Rev. Lett.* **58**, 2802 (1987).
- ⁷⁴ S. Wakimoto, K. Yamada, J. M. Tranquada, C. D. Frost, R. J. Birgeneau, and H. Zhang, *Phys. Rev. Lett.* **98**, 247003 (pages 4) (2007).
- ⁷⁵ S. Wakimoto, H. Zhang, K. Yamada, I. Swainson, H. Kim, and R. J. Birgeneau, *Phys. Rev. Lett.* **92**, 217004 (2004).
- ⁷⁶ T. Thio, T. R. Thurston, N. W. Preyer, P. J. Picone, M. A. Kastner, H. P. Jenssen, D. R. Gabbe, C. Y. Chen, R. J. Birgeneau, and A. Aharony, *Phys. Rev. B* **38**, 905 (1988).
- ⁷⁷ M. A. Kastner, R. J. Birgeneau, T. R. Thurston, P. J. Picone, H. P. Jenssen, D. R. Gabbe, M. Sato, K. Fukuda, S. Shamoto, Y. Endoh, et al., *Phys. Rev. B* **38**, 6636 (1988).
- ⁷⁸ J. B. Torrance, A. Bezing, A. I. Nazzari, T. C. Huang, S. S. P. Parkin, D. T. Keane, S. J. LaPlaca, P. M. Horn, and G. A. Held, *Phys. Rev. B* **40**, 8872 (1989).
- ⁷⁹ H. Takagi, T. Ido, S. Ishibashi, M. Uota, S. Uchida, and Y. Tokura, *Phys. Rev. B* **40**, 2254 (1989).
- ⁸⁰ D. Johnston, *Phys. Rev. Lett.* **62**, 957 (1989).
- ⁸¹ M. Oda, T. Ohguro, H. Matsuki, N. Yamada, and M. Ido, *Phys. Rev. B* **41**, 2605 (1990).
- ⁸² C. Allgeier and J. S. Schilling, *Phys. Rev. B* **48**, 9747 (1993).
- ⁸³ C. H. Pennington, and C. P. Slichter, *Physical properties of high temperature superconductors II*, edited by D. M. Ginsberg, pp.269-368 (1990).
- ⁸⁴ V. Barzykin and D. Pines, *Phys. Rev. Lett.* **96**, 247002 (pages 4) (2006).
- ⁸⁵ B. J. Suh, F. Borsa, J. Sok, D. R. Torgeson, M. Xu, Q. Xiong, and C. W. Chu, *Phys. Rev. B* **54**, 545 (1996).
- ⁸⁶ K. Magishi, Y. Kitaoka, G.-q. Zheng, K. Asayama, T. Kondo, Y. Shimakawa, T. Manako, and Y. Kubo, *Phys. Rev. B* **54**, 10131 (1996).
- ⁸⁷ K. Ishida, K. Yoshida, T. Mito, Y. Tokunaga, Y. Kitaoka, K. Asayama, Y. Nakayama, J. Shimoyama, and K. Kishio, *Phys. Rev. B* **58**, R5960 (1998).
- ⁸⁸ H. Alloul, T. Ohno, and P. Mendels, *Phys. Rev. Lett.* **63**, 1700 (1989).
- ⁸⁹ A. J. Millis, H. Monien, and D. Pines, *Phys. Rev. B* **42**, 167 (1990).
- ⁹⁰ J. C. Campuzano, H. Ding, M. R. Norman, H. M. Fretwell, M. Randeria, A. Kaminski, J. Mesot, T. Takeuchi, T. Sato, T. Yokoya, et al., *Phys. Rev. Lett.* **83**, 3709 (1999).
- ⁹¹ S. H fner, M. A. Hossain, A. Damascelli, and G. A. Sawatzky, arxiv:0706.4282v1 (2007).
- ⁹² A. Damascelli, Z. Hussain, and Z.-X. Shen, *Rev. Mod. Phys.* **75**, 473 (2003).
- ⁹³ G. Deutscher, *Nature* **397**, 410 (1999).
- ⁹⁴ C. Panagopoulos and T. Xiang, *Phys. Rev. Lett.* **81**, 2336 (1998).
- ⁹⁵ K. Tanaka, W. S. Lee, P. H. Lu, A. Fujimori, T. Fujii, Rasdiana, I. Terasaki, D. J. Scalapino, T. P. Devereaux, Z. Hussain, et al., *Science* **314**, 1910 (2006).
- ⁹⁶ M. R. M. R. N. S. S. M. S. Z. Z. L. H. R. A. Kanigel, U. Chatterjee and J. C. Campuzano, arXiv:0708.4099v1. (2007).
- ⁹⁷ P. A. Lee, N. Nagaosa, and X.-G. Wen, *Rev. Mod. Phys.* **78**, 17 (2006).
- ⁹⁸ V. J. Emery and S. A. Kivelson, *Nature* **374**, 436 (1995).